Chapter 6

Iridium-based double perovskites for efficient water oxidation in acid media

ABSTRACT

The development of active, cost-effective and stable anodes for the oxygen evolution reaction (OER) is one of the major challenges for the solar-to-fuel conversion towards sustainable energy generation. IrO2 is the most active catalyst for OER in acid media, and the only one having long-term stability, but it is prohibitively expensive for large-scale applications. The design of new catalysts with lower amounts of the scarce but active and stable iridium is an attractive alternative to overcome this economical constraint. In this work, we report a new type of OER anodes based on iridium double perovskites which contain three times less iridium and exhibit a more than 3-fold higher activity per cm2 of real surface area for OER in acid media compared to IrO2, with more than 90% Faradaic efficiency. We show that these compounds are the most active catalysts for OER in acid media reported to date, according to recently suggested benchmarking criteria.

The content of this chapter is the basis of a patent application, and a manuscript has been submitted for publication: Diaz-Morales O.; Raaijman, S.; Kortlever, R.; Kooyman, P. J.; Wezendonk, T.; Gascon, J.; Fu, W.T. and Koper, M.T.M.

6.1. Introduction

Energy generation by burning fossil fuels has huge environmental effects. The steady increase of the global population, with the concomitant increase in energy needs, requires the development of clean and renewable sources of energy for a sustainable society in the future.[1-3] Solar energy is by far the largest exploitable resource, but its availability is neither temporal nor geographically constant so that its large-scale storage will be a crucial step toward the use of this form of energy as a viable alternative.[2-4] Photo-electrochemical generation of fuels (hydrogen or hydrocarbons) is a promising way to store solar energy. However, the slow kinetics of the anode reaction (water oxidation, or oxygen evolution reaction OER) and the lack of a stable, abundant, and cost-effective OER catalyst limit its large-scale application.[5]

Anodes for OER also find widespread utilization in acid electrolyzers and in technical electrochemistry applications requiring a stable and energy-efficient anode (such as electroplating and electrowinning).[6,7] The current anode material of choice for acid-based industrial operation is TiO_2-stabilized iridium oxide or ruthenium oxide, also known as the Dimensionally Stable Anode (DSA).[6,8-11] Iridium oxide is the most efficient material for the OER in acid media among all transition metal oxides, and the only one having long-term stability.[6,12,13]

In alkaline media, oxides based on earth abundant 3d transition metals such as Ni, Co, Mn and Fe show good stability and activity,[14-18] sometimes even higher than the expensive and scarce IrO_2 and RuO_2, and are typically used as anode materials in alkaline electrolyzers.[19,20] However, the kinetics for hydrogen generation is slower in alkaline media than in acid[21,22]. Furthermore, the electrolytes typically used in alkaline electrolyzers have low conductivities; this causes high Ohmic losses in the device and limits the maximum achievable current to about 0.3 A cm^{-2}, much lower than the values achievable by proton exchange membrane electrolyzers (PEM), which are higher than 1.6 A cm^{-2}.[19,20] Such high current densities are required for large-scale and cost-efficient applications of water electrolysis. Moreover, the diaphragms used to separate the anode and cathode chamber in

the alkaline electrolyzers do not completely prevent the product gases from cross-diffusing, which also compromises the efficiency and safety of these devices[23]. PEM electrolyzers overcome this problem by using proton exchange membranes (*eg.* perfluorinated Nafion® membranes) that are efficient gas separators, but this type of membranes is unsuitable in alkaline media.[24]

Iridium is one of the rarest metals on earth, and its high price makes it unsuitable for large scale application. Therefore, development of active and stable OER catalysts with a lower amount of the expensive but highly active iridium[25,26], in combination with iridium recycling, is an alternative avenue (and may presently well be the most realistic avenue) for the extensive application of hydrogen/hydrocarbon generation in solar energy storage, as well as for the development of cheaper and more efficient anodes for the electrochemical industry.

This work reports on a new class of OER catalysts based on iridium double perovskites which contain three times less iridium and yet exhibit a more than 3-fold higher activity per cm2 of real surface area (see Experimental Section for details) for OER in acid media compared to IrO_2, with a similar stability. We will show that these compounds are the most active catalysts for OER in acid media reported till now, according to recently suggested benchmarking criteria.[18]

Double perovskites are compounds with the generic formula $A_2BB'O_6$, with *A* being a large cation and *B* and *B´* being smaller cations. The crystal structure of the ideal double perovskite is depicted schematically in Figure 1(a), showing the three-dimensional network of corner-shared octahedra BO_6 / $B'O_6$ with the *A* cations located in the cavity composed of 8 BO_6 / $B'O_6$ octahedra.[27-29] A wide range of compounds can be prepared by different combinations of *A*, *B* and *B´* cations, which allows fine tuning of the double perovskites components. This feature is used in our work to obtain insight in the parameters affecting the catalytic activity of the A_2BIrO_6 double perovskites, with *A* = Ba, Sr and *B* = La, Ce, Pr, Nd, Tb, Y.

6.2. Experimental Section

6.2.1. Chemicals

The water used to prepare solutions and clean glassware was deionized and ultrafiltrated with a Millipore Milli-Q system (resistivity = 18.2 MΩ·cm and TOC< 5 ppb). All chemicals used in this work were of high purity (pro analysis grade or superior) and they were used without any further purification. The perchloric acid used for the electrolyte was from Merck (70-72%, EMSURE®).

6.2.2. Synthesis and characterization of the iridium-based catalysts

Ba_2MIrO_6 (M= La, Ce, Pr, Nd, Tb and Y), Sr_2YIrO_6, Sr_2IrO_4 and Pr_3IrO_7 were prepared, respectively, from $BaCO_3$, $SrCO_3$, La_2O_3, CeO_2, Pr_6O_{11}, Nd_2O_3, Tb_4O_7, Y_2O_3 and metallic iridium powder, respectively, in alumina crucibles, using the standard solid-state reactions described in references.[30-33] All reactions were carried out in air and the products were furnace-cooled to room temperature. The powders were intermittently reground during the synthesis.

The suspension of iridium oxide nanoparticles was prepared by hydrolysis of Na_2IrCl_6 in alkaline media at 90 °C, to form $[Ir(OH)_6]^{2-}$ intermediate; the particles were generated by an acid-catalyzed condensation of this intermediate.[34]

X-ray powder diffraction patterns were collected on a Philips X'Pert diffractometer, equipped with the X'Celerator, using Cu-Kα radiation in steps of 0.020º (2θ) with 10 s counting time in the range $10º < 2\theta < 100º$.

6.2.3. Electrochemical experiments

Glassware was cleaned by boiling in a 3:1 mixture of concentrated sulfuric acid and nitric acid to remove organic contaminations, after which it was boiled five times in water. When not in use, the glassware was stored in a solution 0.5 M H_2SO_4 and 1 g/L $KMnO_4$. To clean the glassware from permanganate solution, it was rinsed thoroughly with water and

then immersed in a solution 1:1 of concentrated H_2SO_4 and 30% H_2O_2 to remove the MnO_2 particles, after which it was rinsed with water again and boiled five times in ultrapure water.

The electrochemical measurements were carried out at room temperature in a two compartment electrochemical cell with the reference electrode separated by a Luggin capillary. Measurements were performed using a homemade rotating Pt ring – Au disk electrode (ϕ_{disk} = 4.6 mm) as working electrode, a gold spiral as counter electrode and a reversible hydrogen electrode (RHE) as reference electrode; a platinum wire was connected to the reference electrode through a capacitor of 10 μF, acting as a low-pass filter to reduce the noise in the low current measurements. The electrochemical measurements were controlled with a potentiostat/galvanostat (PGSTAT12, Metrohm-Autolab) and they were performed either with cyclic voltammetry at 0.01 V/s or with potentiostatic steps of 0.02 V every 30 seconds. The latter procedure is referred to as steady-state measurements. Before and between measurements the working electrode was polished with 0.3 μm and 0.05 μm alumina paste (Buehler Limited), subsequently it was ultrasonicated in water for 5 minutes to remove polishing particles. The electrolyte was saturated with air prior to the experiments by bubbling for 20 min with compressed air, with the air first passed through a 6 M KOH washing solution. The rotating ring-disk (RRDE) experiments to measure the faradaic efficiency were carried out with the electrolyte saturated with argon, which was purged through for at least 30 min prior to the experiment and kept passing above the solution during the measurement. For RRDE measurements, the Pt ring was kept at 0.45 V vs. RHE while the disk with the catalyst loaded was scanned at 0.01 V/s in the potential range 1.25 – 1.75 V vs. RHE.

The catalysts were immobilized on the Au disk by drop-casting an ethanol-based ink of the oxides, using Na-exchanged neutral Nafion as binder.[35] The inks were prepared to yield the following final concentrations: 1 mg_{oxide}/mL_{ink} and 0.7 mg_{Nafion}/mL_{ink}.[36] Prior to the preparation, the powders were ground in a mortar to eliminate big clusters. The appropriate amount of ink was drop-casted on the electrode to obtain 15 $\mu g_{oxide}/cm_{disk}^2$ of

loading and this electrode was dried in vacuum; cm_{disk}^2 refers to the geometrical surface area of the Au disk.

The current densities reported in this work were calculated with the electrochemical surface area, obtained from pseudo-capacitance measurements, assuming 60 $\mu F \cdot cm^{-2}$ for the specific capacitance of the double layer.[18,37] The Tafel plots were corrected for the Ohmic resistance of the electrolyte, the resistance was measured by Electrochemical Impedance Spectroscopy and by conductimetry[18] and the value obtained was $24 \pm 1\ \Omega$.

6.3. Results and Discussion

The catalytic activity (measured as the current density) towards OER in 0.1 M $HClO_4$ (pH=1) was studied for iridium-based double perovskites with the same *A*-cation (Ba), but changing the *B* cations (La, Ce, Pr, Nd, Tb and Y). The electrodes were prepared by drop-casting an ethanol-based ink of the double perovskites on a rotating ring-disk electrode and the electrochemical experiments were carried out under rotating conditions (see Experimental section for further details). The structure of the double perovskites was verified by powder XRD and the patterns obtained agree with those reported in the literature,[30,31,38] as shown in Figures E1-E7 in Appendix E. Figure 1b summarizes the measured catalytic activities in the form of Tafel plots and compares it with IrO_2 nanoparticles that have been reported as the activity benchmark for OER in acid media.[18] The observed activity of the IrO_2 nanoparticles compares well with the activity reported previously for similar IrO_2 nanoparticles.[18,39] The current density was obtained by normalizing the measured current with respect to the real oxide surface area, as obtained by pseudo-capacitance measurements, following the procedure suggested by Trasatti and Petrii[37] and further developed by McCrory *et al.*[18] (see Experimental section for further details). This procedure of surface area determination is preferred over the Brunaur-Emmet-Teller (BET) method, based on the physical absorption of a gas on the oxide powder, because it allows us to estimate the active electrochemical surface area that can be very different from the real surface area estimated by the BET physical adsorption method.[37]

All Ir-based double perovskites show a more than 3-fold higher catalytic activity per cm^2 of real surface area towards oxygen evolution compared with the benchmarking IrO_2 nanoparticles. Their activity depends on the lanthanide in the B-site, in the order Ce ≈ Tb < La ≈ Pr < Nd. Substitution of the A-site cation can also affects the catalytic activity as is illustrated in Figure 1c which shows that catalytic activity of Sr_2YIrO_6 is higher compared with its barium equivalent. The iridium double perovskites with strontium and lanthanides were also prepared but we did not manage to prepare pure phases of these compounds. Only Sr_2YIrO_6 formed a single phase, hence it was the only iridium double perovskite with strontium used for the electrochemical characterization of the OER activity.

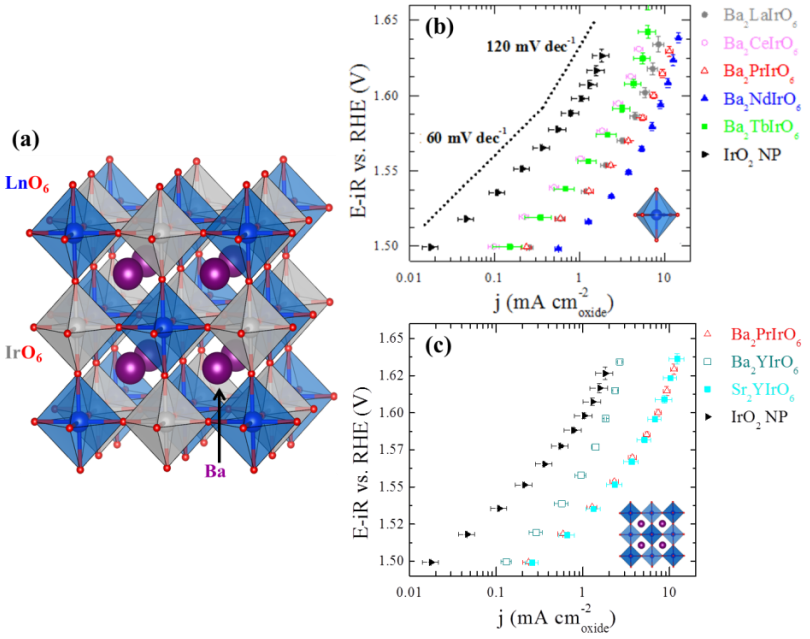

Figure 1. a) Schematic representation of the crystal structure of a generic Ba_2LnIrO_6 double perovskite. b) Catalytic activity to OER in 0.1 M $HClO_4$ of Ir-based double perovskites with A = Ba and with different lanthanides, compared to the benchmark activity IrO_2 nanoparticles; the dashed line shows Tafel slopes of 60 and 120 mV/dec, to guide the eye. c) Effect of the lanthanides and barium substitution on the catalytic activity for water oxidation in 0.1 M $HClO_4$ M of the Ir-based double perovskite. Measurements were performed in hydrodynamic conditions at 1500 RPM.

Both the IrO_2 nanoparticles and the iridium-based double perovskites show two values for the Tafel slope, *ca.* 60 mV/dec between 1.5 and 1.6 V vs. RHE and 120 mV/dec at potentials higher than 1.6 V (numerical values are given in table E1 in Appendix E). This feature has been reported previously for IrO_2 and was explained by a change in the mechanism for OH adsorption, which is thought to be the rate determining step for oxygen evolution on iridium oxide.[40,41] We note, however, that the Tafel slope measured at high electrode potentials for Ba_2YIrO_6 (196 $\pm$ 23 mV/dec) markedly deviates from the values for the iridium-based double perovskites (*ca.* 120 mV/dec).

The catalytic activity towards OER sensitively depends on the crystal structure of the iridium-based catalyst. Figure 2a-b compares the activity of the Ba_2PrIrO_6 and Sr_2YIrO_6 double perovskites with Sr_2IrO_4 and Pr_3IrO_7 (XRD for these compounds are shown in Figure E8-E9 in Appendix E). The catalytic activity of Sr_2IrO_4 is quite similar to that of Sr_2YIrO_6 (see Figure 2a); whereas that of Pr_3IrO_7 is 10-fold lower than the Ba_2PrIrO_6, though comparable to the activity of the IrO2 nanoparticles. The structure of Sr_2IrO_4 and Pr_3IrO_7 also contain the corner-shared IrO_6 octahedra, but differ from that of the double perovskite in the network arrangement. The Sr_2IrO_4 forms two-dimensional (2D) perovskite-like layers,[32,42] separated by a rock salt layer of SrO (see Figure 2c), whereas in the Pr_3IrO_7, the IrO_6 octahedra are linked by sharing the corner oxygen and form one-dimensional (1D) chains[33] (see Figure 2d).

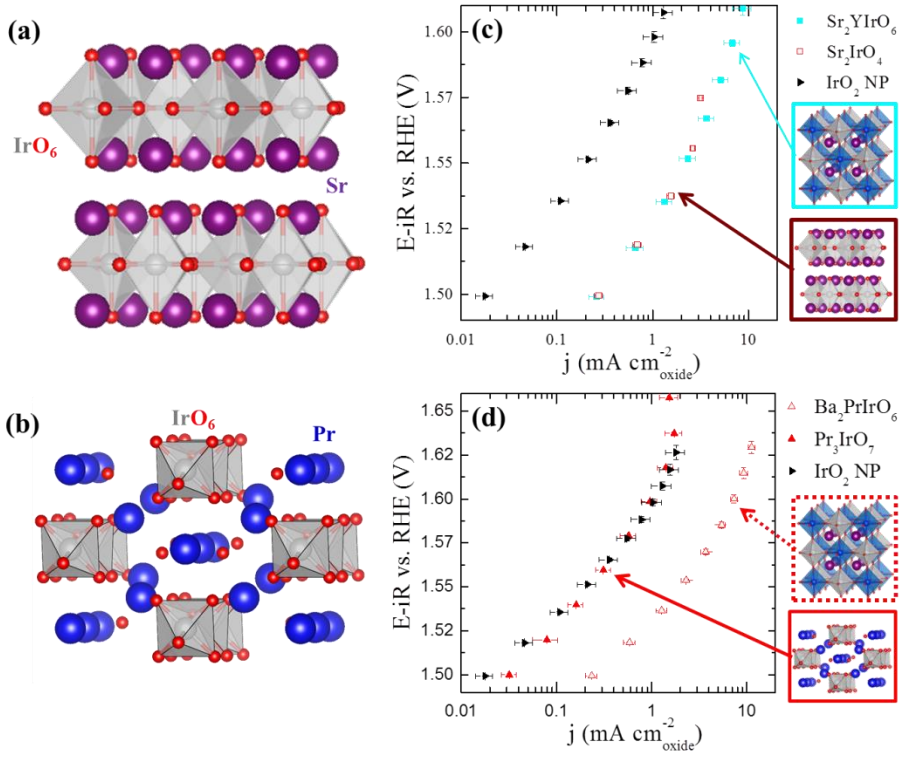

Figure 2. a) Crystal structure of Sr_2IrO_4, showing the 2D network of corner-shared octahedra. b) Crystal structure of Pr_3IrO_7, showing the 1D network of corner-shared octahedra. c) Catalytic activity for OER in 0.1 M $HClO_4$ M of Sr_2YIrO_6 double perovskites in comparison with Sr_2IrO_4 perovskite-like structure. d) Catalytic activity for water oxidation in 0.1 M $HClO_4$ of Ba_2PrIrO_6 double perovskites in comparison with Pr_3IrO_7 fluorite-like structure. Measurements were performed at steady-state conditions at 1500 RPM. The benchmark activity of IrO_2 nanoparticles is shown as benchmark.

The results shown in Figure 2c-d suggest that the 2D arrangement of corner-shared octahedra is the minimal condition to obtain the enhanced catalytic activity of the iridium-based perovskite-like compounds with respect to conventional IrO_2. However, stability under the anodic working conditions is observed only with the extended 3D arrangement of corner-share octahedral of the double perovskites, as illustrated in the voltammetry data shown in Figure E10 in Appendix E. The Sr_2IrO_4 is certainly catalytically active towards

OER in the first cycle(s), but it tends to deactivate after a number of oxygen evolution cycles in the acid environment.

The electrochemical stability of the Ir-based double perovskites was assessed by galvanostatic electrolysis, in a manner similar to the approach reported by the JCAP group.[18] The experiment was performed by applying 10 mA cm_{disk}^{-2} for 1 h (cm_{disk}^{-2} refers to the geometrical surface area of the electrode), and the Ohmic drop-corrected overpotential for OER after 1 h of electrolysis is plotted versus the overpotential measured at the beginning of the experiment (t = 0 s). Figure 3 summarizes the results obtained from these experiments. The stability of IrO_2 nanoparticles is presented for comparison. The diagonal dashed line represents the expected response of a stable catalyst.

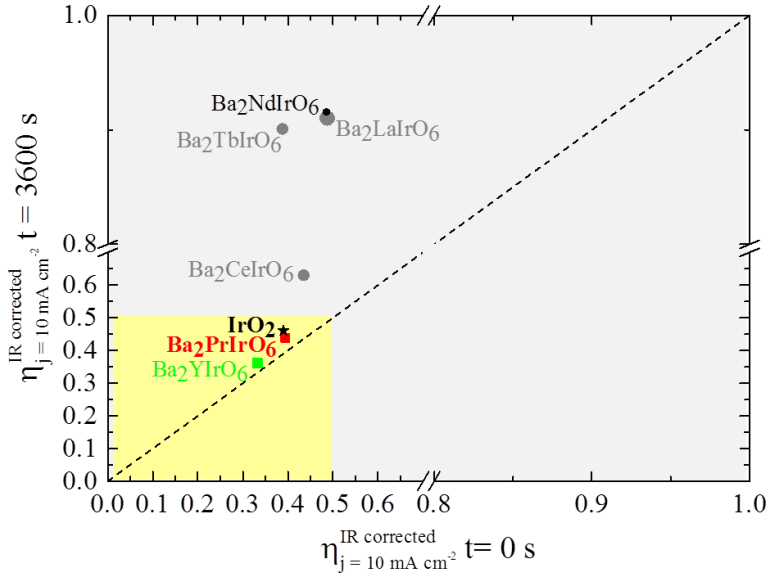

Figure 3. Illustration of the stability of the Ir-based double perovskites and IrO_2 nanoparticle under anodic condition for electrochemical water oxidation in 0.1 M $HClO_4$. The Ohmic drop-corrected overpotential measured after 1 h of galvanostatic electrolysis at 10 mA cm_{disk}^{-2} in hydrodynamic conditions (ω = 1500 RPM) is plotted as a function of the initial overpotential.

The results in Figure 3 show that Ba_2PrIrO_6 and Ba_2YIrO_6 are electrochemically stable, and show similar stability as the IrO_2, which is the state-of-the-art catalyst for OER in acid. The electrochemical stability of these compounds can be illustrated by a plot of Ohmic drop-corrected overpotential as a function of time obtained from the galvanostatic electrolysis (see Figure E10 in Appendix E). During such a time-dependent electrolysis, the Ba_2PrIrO_6 and Ba_2YIrO_6 compounds show even better stability in terms of overpotential than the IrO_2 catalyst. The lanthanum, neodymium and terbium- containing double perovskites are also very active towards OER in acid media according to the JCAP benchmarking, with an overpotential for 10 mA cm^{-2} in the range 0.4 – 0.5 V (see Figure 3). However, they lose their activity after 1 h of galvanostatic electrolysis as expressed by their higher OER overpotentials after 1 h of electrolysis.

In order to assess the structural stability of the Ir-based double perovskites, Ba_2PrIrO_6 was characterized by TEM and XRD after 48 h of leaching treatment in harsh media, namely 0.1 M $HClO_4$ and in 0.1 M $HClO_4$ + 4 M H_2O_2. The Ba_2PrIrO_6 compound was selected for these experiments because it was one of the compounds that showed to be electrochemically stable (see Figure 3), hence we wanted to assess whether it is also structurally stable. The open-circuit potentials of the Ba_2PrIrO_6 double perovskite in 0.1 M $HClO_4$ solution and in 0.1 M $HClO_4$ + 4 M H_2O_2 solution were measured to be 1.3 and 1.1 V vs. RHE, respectively. Therefore the characterization of the powder leached in these two solutions should give a hint about the stability of the double perovskite in acid at the onset of the OER. The TEM images in Figures E11 – E16 in Appendix E show that all the pristine iridium-based double perovskites consist of rather large particles (*ca.* 0.5 – 2 μm), consistent with the sharp lines in XRD pattern (see Figure E1-E7 in Appendix E). The particle size of the Ba_2PrIrO_6 powders leached in 0.1 M $HClO_4$ and 0.1 M $HClO_4$ + 4 M H_2O_2 (Figures E17 – E18 in Appendix E) and the XRD pattern (Figure E19 in Appendix E) remains virtually the same. This shows that the crystal structure of the double perovskite is preserved during the leaching treatment. However, there are a higher number of smaller particles (particle size below 200 nm) in the samples that were leached than in the pristine compound (see Figure E13 in comparison with Figures E17 – E18 in Appendix E). This

suggest that Ba_2PrIrO_6 either cleaves or partially dissolves during the leaching treatment but this process seems to be slow, therefore the average particle size is still large so that no significant broadening is observed in the XRD pattern (see Figure E19 in Appendix E).

We also characterized the surface composition of the pristine and leached samples of the Ba_2PrIrO_6 double perovskite by means of X-ray photoelectron spectroscopy (XPS). The results of this analysis are summarized in Figure E20 and table E2 in Appendix E. The main conclusion derived from this study is that the surface of the double perovskite is not stable upon the acid and the oxidative treatment. XPS results indicate that surface enrichment in iridium occurs upon both leaching treatments of Ba_2PrIrO_6, whereas the barium surface contribution reduces *ca.* 3-fold after leaching in 0.1 M $HClO_4$ and 4-fold after treatment with 0.1 M $HClO_4$ + 4 M H_2O_2, with respect to the pristine compound. Regarding the oxidation state of iridium in the pristine and treated samples, our results show that the surface iridium sites contain a mixture of Ir(IV) and Ir(V), and become enriched in Ir(V) upon the leaching treatments (see Figure E21 in Appendix E).

The leaching of the components of the Ba_2PrIrO_6 double perovskite during electrochemical experiments for oxygen evolution was also assessed by elemental analysis of the electrolyte after electrolysis experiments of one hour at constant electrode potential (see table E3 in Appendix E). The analysis indicates that approximately 10% of Ba and Pr are leached out of the double perovskites in the potential region 1.45 – 1.55 V vs. RHE; however, a negligible amount of iridium dissolves (less than 1%). These results are consistent with the evidence from XPS, indicating that barium and praseodymium are superficially removed at oxidative potentials but that these surface changes do not affect the bulk of the double perovskite, and therefore do not change the XRD pattern, and do not impact on the electrochemical stability of the perovskite as evaluated by the JCAP protocol.

Summarizing, the galvanostatic electrolysis results and the characterization by TEM and XRD show that the bulk of the Ba_2PrIrO_6 double perovskite is electrochemically and structurally stable in acid environment under oxidative conditions. However, the XPS and elemental electrolyte analyses indicate that the surface of the compound changes under

oxidative conditions, becoming enriched in iridium (which tends to be converted to the Ir(V) state) with approximately 10% of Ba and Pr dissolved from the double perovskite.

Finally, we measured the Faradaic efficiency of Ba_2PrIrO_6 towards OER in 0.1 M $HClO_4$ in a rotating ring-disk electrode (RRDE) configuration. The result of this measurement is shown in Figure E22 in the Appendix E and shows that Ba_2PrIrO_6 has high efficiency towards water oxidation, higher than 90% at 1.50 V vs. RHE (0.27 V of overpotential). The Faradaic efficiency appears to decrease with the more anodic electrode potential, which can be explained by the large current for oxygen evolution at $E \geq 1.6$ V vs. RHE, leading to the formation of oxygen bubbles which reduces the detection efficiency on the ring. The double perovskites have very high tendency to bubble formation (due to their high activity) even at low OER overpotentials, which reduces the amount of dissolved O_2 detected at the ring and therefore the reported Faradaic efficiency. This can explain the apparent 10% efficiency loss at 0.27 V of overpotential.

Regarding the high activity measured for the Ir-based double perovskites, Calle-Vallejo *et al.*[43] showed that the oxygen adsorption energy on ABO_3 simple perovskites (with B = Sc, Ti, V, Cr, Mn, Fe, Co, Ni, Cu and A = La, Y) is slightly lower for the yttrium based perovskites and they suggest this might be due to strains in the crystal lattice caused by the smaller Y, in comparison with La. This was also observed for the 3d transition metal perovskites with A = Ba, Sr, strontium-based perovskites showing slightly weaker binding energy than the barium equivalent. Since the IrO_2 has been reported to bind oxygen too strongly to be a truly optimal catalyst,[44,45] the lattice strain caused by substitution of smaller lanthanides or yttrium could weaken the oxygen adsorption energy and therefore improve the catalytic activity of the iridium-based double perovskites in comparison with iridium oxide. The catalytic activity of Ba_2CeIrO_6 shows an additional effect related with the tetravalent oxidation state of the iridium centers;[31,38] this increases the binding energy of adsorbates[43] and may explain why the cerium compound is the least active in the series. In addition, the observed surface leaching may also contribute to the enhancement of the OER catalytic activity of the perovskite surface by leaving behind highly active iridium centers.

6.4. Conclusions

We have reported a new family of iridium-based double-perovskite electrocatalysts with superior activity for water oxidation in acid media. Compared to IrO_2, the state-of-the art benchmarking catalyst, these compounds contains three times less iridium, and exhibit a more than 3-fold higher catalytic activity per cm^2 of real surface area for the oxygen evolution reaction. Our results show that a 3D network of corner-shared octahedra is a necessary prerequisite for the catalytic activity enhancement of the iridium-based double perovskites and for their chemical stability under anodic working conditions. Our findings regarding the effect of the A and B-site cations on the catalysis towards water splitting of the iridium based double perovskite suggest that the activity of these compounds might be further improved by carefully selecting the cations at those sites. Our strategy could also be extended to enhance the catalytic activity and chemical stability of ruthenium-containing compounds, with lower content of ruthenium compared with RuO_2.

6.5. Acknowledgments

This work was also supported by the Netherlands Organization for Scientific Research (NWO) and in part by the BioSolar Cells open innovation consortium, supported by the Dutch Ministry of Economic Affairs, Agriculture and Innovation. Dr. W.T. Fu is kindly acknowledged for his assistance with the synthesis of the double perovskites and their XRD characterization. Dr. P. Kooyman and R. Kortlever are acknowledged for the TEM characterization. Thanks to Prof. J. Gascon and T. Wezendonk for the XPS analysis. Special thanks to S. Raaijman for his assistance with the synthesis, XRD and electrochemical characterization of double perovskites.

REFERENCES

(1) Olah, G. A.; Prakash, G. K.; Goeppert, A. *J. Am. Chem. Soc.* **2011**, *133*, 12881.

(2) Bensaid, S.; Centi, G.; Garrone, E.; Perathoner, S.; Saracco, G. *ChemSusChem* **2012**, *5*, 500.

(3) Crabtree, G. W.; Dresselhaus, M. S.; Buchanan, M. V. *Physics Today* **2004**, *57*, 39.

(4) Lewis, N. S.; Nocera, D. G. *Proceedings of the National Academy of Sciences of the United States of America* **2006**, *103*, 15729.

(5) Koper, M. T. M. *Journal of Electroanalytical Chemistry* **2011**, *660*, 254.

(6) Hayfield, P. C. S. *Platinum Metals Rev.* **1998**, *42*, 116.

(7) Schmachtel, S.; Toiminen, M.; Kontturi, K.; Forsen, O.; Barker, M. H. *J. Appl. Electrochem.* **2009**, *39*, 1835.

(8) da Silva, L. A.; Alves, V. A.; da Silva, M. A. P.; Trasatti, S.; Boodts, J. F. C. *Canadian Journal of Chemistry-Revue Canadienne De Chimie* **1997**, *75*, 1483.

(9) Depauli, C. P.; Trasatti, S. *J. Electroanal. Chem.* **1995**, *396*, 161.

(10) Trasatti, S. *Electrochim. Acta* **2000**, *45*, 2377.

(11) Hu, J. M.; Zhang, J. Q.; Cao, C. N. *Int. J. Hydrogen Energy* **2004**, *29*, 791.

(12) Matsumoto, Y.; Sato, E. *Mater. Chem. Phys.* **1986**, *14*, 397.

(13) Antolini, E. *ACS Catal.* **2014**, *4*, 1426.

(14) Oliva, P.; Leonardi, J.; Laurent, J. F.; Delmas, C.; Braconnier, J. J.; Figlarz, M.; Fievet, F.; Guibert, A. d. *J. Power Sources* **1982**, *8*, 229.

(15) Corrigan, D. A.; Bendert, R. M. *Journal of The Electrochemical Society* **1989**, *136*, 723.

(16) Suntivich, J.; May, K. J.; Gasteiger, H. A.; Goodenough, J. B.; Shao-Horn, Y. *Science* **2011**, *334*, 1383.

(17) Grimaud, A.; May, K. J.; Carlton, C. E.; Lee, Y. L.; Risch, M.; Hong, W. T.; Zhou, J.; Shao-Horn, Y. *Nat Commun* **2013**, *4*, 2439.

(18) McCrory, C. C.; Jung, S.; Peters, J. C.; Jaramillo, T. F. *Journal of the American Chemical Society* **2013**, *135*, 16977.

(19) Carmo, M.; Fritz, D. L.; Mergel, J.; Stolten, D. *International Journal of Hydrogen Energy* **2013**, *38*, 4901.

(20) Holladay, J. D.; Hu, J.; King, D. L.; Wang, Y. *Catalysis Today* **2009**, *139*, 244.

(21) Markovic, N. M.; Sarraf, S. T.; Gasteiger, H. A.; Ross, P. N. *J. Chem. Soc., Faraday Trans.* **1996**, *92*, 3719.

(22) Sheng, W.; Gasteiger, H. A.; Shao-Horn, Y. *J. Electrochem. Soc.* **2010**, *157*, B1529.

(23) Schröder, V.; Emonts, B.; Janßen, H.; Schulze, H. P. *Chemical Engineering & Technology* **2004**, *27*, 847.

(24) Zeng, K.; Zhang, D. *Prog. Energy Combust. Sci.* **2010**, *36*, 307.

(25) Hu, W.; Zhong, H.; Liang, W.; Chen, S. *ACS Applied Materials & Interfaces* **2014**, *6*, 12729.

(26) Nong, H. N.; Gan, L.; Willinger, E.; Teschner, D.; Strasser, P. *Chem. Sci.* **2014**, *5*, 2955.

(27) Howard, C. J.; Stokes, H. T. *Acta Crystallographica Section A* **2005**, *61*, 93.

(28) Howard, C. J.; Kennedy, B. J.; Woodward, P. M. *Acta Crystallographica Section B* **2003**, *59*, 463.

(29) Howard, C. J.; Stokes, H. T. *Acta Crystallographica Section B* **2004**, *60*, 674.

(30) Fu, W. T.; Ijdo, D. J. W. *J. Alloys Compd.* **2005**, *394*, L5.

(31) Fu, W. T.; Ijdo, D. J. W. *J. Solid State Chem.* **2005**, *178*, 1312.

(32) Huang, Q.; Soubeyroux, J. L.; Chmaissem, O.; Sora, I. N.; Santoro, A.; Cava, R. J.; Krajewski, J. J.; Peck Jr, W. F. *J. Solid State Chem.* **1994**, *112*, 355.

(33) Vente, J. F.; Ijdo, D. J. W. *Mater. Res. Bull.* **1991**, *26*, 1255.

(34) Zhao, Y.; Hernandez-Pagan, E. A.; Vargas-Barbosa, N. M.; Dysart, J. L.; Mallouk, T. E. *The Journal of Physical Chemistry Letters* **2011**, *2*, 402.

(35) Diaz-Morales, O.; Hersbach, T. J. P.; Hetterscheid, D. G. H.; Reek, J. N. H.; Koper, M. T. M. *J. Am. Chem. Soc.* **2014**, *136*, 10432.

(36) Suntivich, J.; Gasteiger, H. A.; Yabuuchi, N.; Shao-Horn, Y. *J. Electrochem. Soc.* **2010**, *157*, B1263.

(37) Trasatti, S.; Petrii, O. A. *Journal of Electroanalytical Chemistry* **1992**, *327*, 353.

(38) Wakeshima, M.; Harada, D.; Hinatsu, Y. *J. Mater. Chem.* **2000**, *10*, 419.

(39) Lee, Y.; Suntivich, J.; May, K. J.; Perry, E. E.; Shao-Horn, Y. *The Journal of Physical Chemistry Letters* **2012**, *3*, 399.

(40) Hu, J.-M.; Zhang, J.-Q.; Cao, C.-N. *International Journal of Hydrogen Energy* **2004**, *29*, 791.

(41) Dau, H.; Limberg, C.; Reier, T.; Risch, M.; Roggan, S.; Strasser, P. *ChemCatChem* **2010**, *2*, 724.

(42) Beznosikov, B. V.; Aleksandrov, K. S. *Crystallography Reports* **2000**, *45*, 792.

(43) Calle-Vallejo, F.; Inoglu, N. G.; Su, H.-Y.; Martinez, J. I.; Man, I. C.; Koper, M. T. M.; Kitchin, J. R.; Rossmeisl, J. *Chemical Science* **2013**, *4*, 1245.

(44) Rossmeisl, J.; Qu, Z. W.; Zhu, H.; Kroes, G. J.; Nørskov, J. K. *J. Electroanal. Chem.* **2007**, *607*, 83.

(45) Man, I. C.; Su, H.-Y.; Calle-Vallejo, F.; Hansen, H. A.; Martínez, J. I.; Inoglu, N. G.; Kitchin, J.; Jaramillo, T. F.; Nørskov, J. K.; Rossmeisl, J. *ChemCatChem* **2011**, *3*, 1159.